corrosion and materials degradation

MDPI

Article

Cyclic Loading of Metallic Glasses Prepared Using Cryogenic Treatments

Nicolás Amigo

Departamento de Física, Facultad de Ciencias Naturales, Matemática y del Medio Ambiente, Universidad Tecnológica Metropolitana, Las Palmeras 3360, Ñuñoa, Santiago 7800003, Chile; namigo@utem.cl

Abstract: This study investigates the degradation of mechanical properties in CuZr metallic glasses (MGs) under cyclic loading using molecular dynamics simulations. Both as-cast (AC) and cryogenically thermal-cycled (TC) samples with $Cu_{36}Zr_{64}$ and $Cu_{64}Zr_{36}$ compositions were analyzed. Results show that cyclic loading significantly degrades Young's modulus, ultimate tensile stress, and toughness, with most pronounced reductions occurring in the initial cycles. TC samples exhibit improved ductility and stability compared to AC samples. In contrast, AC samples demonstrate greater initial strength but faster degradation. Cu-rich samples maintain higher strength but degrade similarly to Cu-poor samples. The AC Cu-rich sample experiences more localized deformation and delayed degradation, while TC and AC Cu-poor samples quickly reach a steady state. These findings highlight the influence of atomic composition and thermal treatments on the mechanical performance and degradation behavior of MGs.

Keywords: cyclic loading; mechanical properties; metallic glasses; molecular dynamics

Citation: Amigo, N. Cyclic Loading of Metallic Glasses Prepared Using Cryogenic Treatments. *Corros. Mater. Degrad.* **2024**, *5*, 439–449. https://doi.org/10.3390/cmd5040020

Academic Editors: Patricia Jovičević-Klug, J. Manoj Prabhakar and Matic Jovičević-Klug

Received: 18 September 2024
Revised: 24 September 2024
Accepted: 25 September 2024
Published: 26 September 2024

1. Introduction

Metallic glasses (MGs), characterized by their amorphous structure and lack of crystalline defects, exhibit exceptional mechanical properties, such as high strength, elasticity, and wear resistance [1–4]. However, under cyclic loading conditions, MGs are prone to mechanical degradation, leading to embrittlement, reduced ductility, and eventual failure [5–7]. Unlike crystalline alloys, where fatigue mechanisms are well understood through dislocation movements, the absence of long-range atomic order in MGs complicates the understanding of their fatigue behavior.

Extensive research has been conducted on the effects of cyclic loading on the mechanical properties of MGs, with a focus on fatigue-induced shear banding, structural relaxation, and rejuvenation. Some authors have discussed the relationship between cyclic loading, fatigue, and the initiation and evolution of shear bands, indicating that various factors play key roles in the mechanical response, such as atomic composition, temperature, and cyclic frequency, among others [6,8]. Moreover, cyclic loading can lead to partial nanocrystallization [9] or the precipitation of secondary phases [10], adding additional complexities to the problem. Cyclic loading has also been employed as a technique to achieve rejuvenation or aging. Depending on the cycling parameters, either increased or reduced free volume can be obtained, ultimately dictating the mechanical behavior [11–13]. Here, molecular dynamics (MD) simulations serve as a valuable tool for exploring the atomistic mechanisms in detail. In this regard, it has been revealed that the strain amplitude is critical for determining plastic deformation in CuZrMGs subjected to cyclic loading [14,15]. Furthermore, shear band (SB) initiation can be retarded when the strain amplitude is well below the ultimate tensile strength [16]. The changes in plastic behavior can be attributed to variations in the local atomic structure during cyclic loading. As reported in previous works, some Voronoi polyhedra are more prone to atomic mobility, while full icosahedra are less sensitive to mobility [17]. Interestingly, it has been reported that Voronoi polyhedra

populations do not vary significantly during cyclic loading [14,18]. Thus, the study of MGs subjected to cyclic loading is a complex task, with many variables influencing the mechanical behavior.

This study aims to investigate the mechanisms underlying the degradation of mechanical properties in CuZr MGs under cyclic loading using MD simulations. Samples prepared via cryogenic thermal treatments were subjected to cyclic loading and their mechanical performance was compared to that of as-cast samples. Two different atomic compositions were considered: $Cu_{36}Zr_{64}$ and $Cu_{64}Zr_{36}$. The variation in mechanical properties, plastic deformation, and structural characterization as a function of the number of cycles was explored.

2. Materials and Methods

2.1. Modeling and Software

Interactions between atomic species were modeled using the interatomic potential developed by Mendelev et al. [19]. Various studies have demonstrated that this potential provides in-depth descriptions of both structural and mechanical properties [20–23]. MD simulations were performed using the LAMMPS software (LAMMPS 3 March 2020, https://www.lammps.org (accessed on 1 September 2024)) [24,25] with an integration timestep of 1 fs.

2.2. Preparation of the Metallic Glasses

CuZrMG samples were prepared from a B2-CuZr structure composed of 72,000 atoms. Two different atomic compositions were obtained by randomly replacing Cu atoms: $Cu_{36}Zr_{64}$ and $Cu_{64}Zr_{36}$ MGs. Relaxation was then conducted at 2500 K and zero pressure for 10 ns using periodic boundary conditions and the NPT ensemble. Both samples were subsequently cooled to 400 K at a cooling rate of 10^{13} K/s in the intervals of 2500–900 K and 650–400 K, while a cooling rate of 10^{10} K/s was employed in the interval of 900–650 K. As noted in previous works, the most significant physics related to glass transition phenomena occur near the glass transition temperature T_g, which is in the range of 700–800 K for CuZr systems. Therefore, the cooling rates outside this range are less relevant [26,27]. After quenching the samples, relaxation was carried out for 1 ns at zero pressure. The final dimensions of the samples were $33.0 \times 19.7 \times 1.9$ nm^3 for the $Cu_{36}Zr_{64}$ MG and $32.0 \times 19.2 \times 1.9$ nm^3 for $Cu_{64}Zr_{36}$ MG. These samples are referred to as Cu_{36} AC and Cu_{64} AC, respectively, where AC stands for as-cast.

2.3. Cryogenic Treatments

Cryogenic thermal treatments were performed to obtain samples in a higher energy state. Following the work of Shang et al. [28], thermal cycling treatments were adopted. Each cycle comprised four stages: reduction of temperature from 400 K to 1 K at 2.5×10^{14} K/s, relaxation for 0.1 ns, increase of temperature up to 400 K at 2.5×10^{14} K/s, and relaxation for 0.01 ns. Each cycle was repeated 60 times at zero pressure. Additional details can be found in the work of Amigo [29]. This procedure was conducted for both $Cu_{36}Zr_{64}$ and $Cu_{64}Zr_{36}$ MGs, followed by relaxation at 300 K for 1 ns. These samples are referred to as Cu_{36} TC and Cu_{64} TC, respectively, where TC stands for thermal-cycling.

2.4. Cyclic Loading

Cyclic tensile loading was conducted to assess the mechanical performance of the as-cast and thermal-cycling samples. For this purpose, mechanical deformation was applied by rescaling the atomic positions at 10^8 s^{-1} up to a strain of 0.12 in the x-direction, while keeping the y and z-directions at zero pressure and the sample at 300 K. Unloading was then performed by reducing the pressure in the x-direction to zero. This procedure was repeated five times, resulting in five load–unloading cycles.

2.5. Diagnostic Tools

Structural characterization was performed using Voronoi polyhedra analysis. A Voronoi polyhedron is described by five indices: $\langle n_3, n_4, n_5, n_6 \rangle$, where n_i represents the number of i-edged faces. The five-fold local symmetry (LFFS) was calculated to analyze the fraction of pentagons and the nearest-neighbor atoms. It was determined as $d_5 = n_5 / \sum n_i$ [30,31].

Quantification of plasticity was performed using the atomic strain [32] available in OVITO [33]. The degree of shear localization was calculated as [34]

$$\psi = \sqrt{\frac{1}{N} \sum_{i=1}^{N} (\eta_i - \eta_{ave})^2}, \quad (1)$$

where N is the total number of atoms, η_i is the von Mises strain of atom i, and η_{ave} is the average von Mises strain. The deformation participation ratio (ϕ) was determined as [35,36]

$$\phi = \frac{N^{\eta > 0.2}}{N_t}, \quad (2)$$

where $N^{\eta > 0.2}$ is the number of atoms with von Mises strain greater than 0.2 and N_t is the total number of atoms.

3. Results and Discussion

3.1. Atomic Structure Inspection

Cryogenic thermal cyclic treatments have been shown to induce rejuvenation in CuZrMGs [28,29]. To further explore this, Voronoi analysis was performed on both AC and TC samples, with the resulting populations shown in Figure 1. As observed, cryogenic treatments lead to lower populations of densely-packed polyhedra, particularly in the Cu-rich samples, where the $\langle 0, 0, 12, 0 \rangle$ full icosahedra exhibit the most significant reduction. This indicates that cryogenic treatments are an effective mechanism for reducing the fraction of icosahedra-like polyhedra. The populations of these polyhedra are crucial, as they form the backbone of the MG matrix, governing its response to mechanical deformation and establishing structure–property relationships, as reported in the literature [37–40].

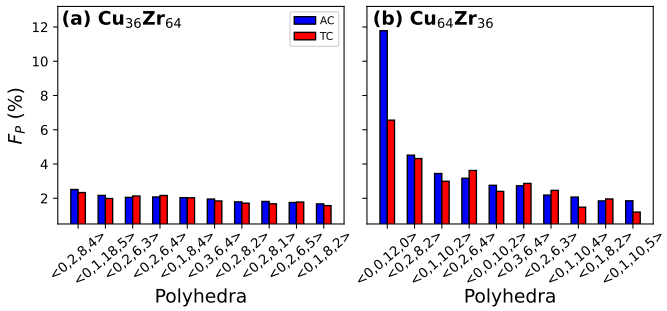

Figure 1. The ten largest populations of voronoi polyhedra for the AC and TC samples.

3.2. Stress–Strain Curves

All samples were subjected to cyclic loading to assess their mechanical performance. The resulting stress–strain curves are shown in Figure 2. When comparing both atomic compositions, the Cu-rich samples exhibit enhanced strength, which is in good agreement with previous studies. It has been reported that Cu species induce the formation of denser structures, leading to increased stiffness [41–44]. Regarding the effect of cryogenic thermal treatments, the TC samples display reduced strength compared to their as-cast counterparts. In the works of Shang et al. [28] and Amigo [29], it was shown that cryogenic treatments under certain conditions can promote rejuvenation in MGs by increasing free volume and driving the samples to higher energy states. Both phenomena contribute to more

homogeneous deformation, thereby improving ductility. When analyzing the cyclic loading behavior, the AC samples exhibit higher stress peaks during the first cycle, followed by a pronounced drop in stress, suggesting the formation of SBs. In subsequent cycles, the stress converges to a steady-state value, which is more prominent in the Cu-poor samples. For the TC samples, all cycles are very similar, indicating that a steady state is rapidly achieved during cyclic loading. Finally, it is interesting to note that the effect of thermal treatments leads to tensile behavior similar to that of samples rejuvenated by elastic cyclic loading [11,12].

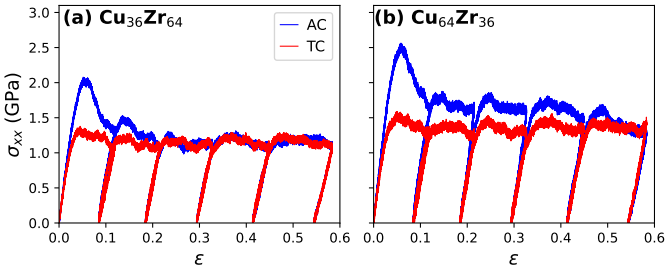

Figure 2. Stress–strain curves for the cyclic loading. AC and TC correspond to as-cast and thermal-cycling samples, respectively.

3.3. Mechanical Properties

To quantify the mechanical response of the samples, the Young's modulus (E), ultimate tensile stress (σ_{uts}), and toughness (u_t) were calculated for each cycle. The Young's modulus was determined as the slope of the linear regime, the ultimate tensile stress as the maximum stress within the 0.00–0.06 strain interval in each cycle, and the toughness as the area under the curve within the 0.00–0.12 strain interval. All values are shown in Figure 3 as a function of the number of cycles. In all cases, a negative trend is observed with the increasing number of cycles, indicating a degradation of the mechanical properties. The Young's modulus exhibits a consistent decrease, while both σ_{uts} and u_t show a steep drop during the first three cycles, followed by a more gradual decline in the fourth and fifth cycles. This reflects the steady-state behavior observed in the stress–strain curves. Additionally, the decreasing toughness values indicate that the materials have a reduced capacity to store deformation energy, making them more prone to failure. When comparing the AC and TC samples for a given atomic composition, the AC MGs show higher values for E, σ_{uts}, and u_t than their TC counterparts, as reported in previous studies on rejuvenation through cryogenic thermal cycling treatments [29]. However, from the third cycle onward, the mechanical properties of both AC and TC samples begin to converge, a trend that is more pronounced in the Cu-poor samples. Therefore, cyclic loading drives the TC samples to structural states similar to those of the AC samples.

The degree of degradation of the mechanical properties was quantified by calculating the percentage difference of each property as $\Delta y = (y_{5th} - y_{1st})/y_{1st} \times 100\%$, where y_{5th} and y_{1st} correspond to a given property calculated in the fifth and first cycles, respectively. The resulting values are shown in Figure 4. The Young's modulus exhibits the largest degradation when considering all four samples together. However, when inspecting the samples separately, large degradation is observed for σ_{uts} and u_t in the AC MGs. In contrast, both properties show smaller degrees of degradation (5–10%) in the TC MGs. Thus, while all cases exhibit statistically significant degradation (above 5%), the AC samples display the most pronounced variations, and the Young's modulus is strongly affected in all cases.

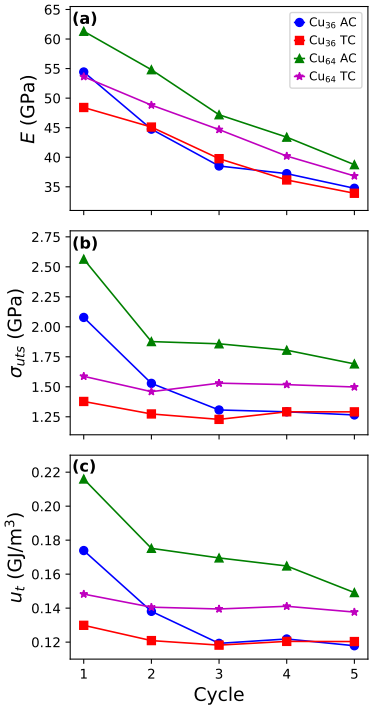

Figure 3. (**a**) Young's modulus, (**b**) ultimate tensile stress, (**c**) and toughness calculated in each cycle for each sample.

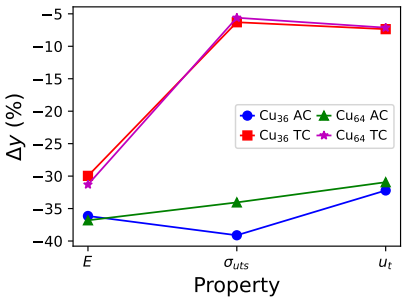

Figure 4. Percentage difference of each mechanical property between the first and last cycle.

3.4. Plastic Behavior

The plastic response of the samples was explored using atomic shear strain. The resulting fields are displayed in Figure 5, showing the final state of each sample during the first, third, and fifth cycles. As expected from the rejuvenation treatments, the TC MGs exhibit more homogeneous deformation due to the nucleation of shear transformation zones (STZs) throughout the glass matrix, whereas the AC MGs show plasticity dominated by SB nucleation [45–47]. However, as cyclic loading progresses, most of the glass matrix experiences severe deformation, except in the AC Cu-rich sample, where plasticity remains dominated by heavily localized SBs. As reported in previous studies, plastic deformation induced by tensile loading promotes increased free volume [48,49]. Consequently, as the MGs gradually accumulate free volume with each cycle, the Young's modulus undergoes continuous degradation during cyclic loading. Moreover, the presence of pre-existing STZs/SBs at the beginning of each cycle facilitates the nucleation of additional plastic events, leading to reductions in the ultimate tensile stress and toughness of the samples until a steady state is reached. It is important to note that in this work, complete plastic deformation occurs earlier than in other studies, due to the higher strain applied here in each cycle (up 0.12 strain) compared to other works (up to 0.06–0.10 strain) [14,16].

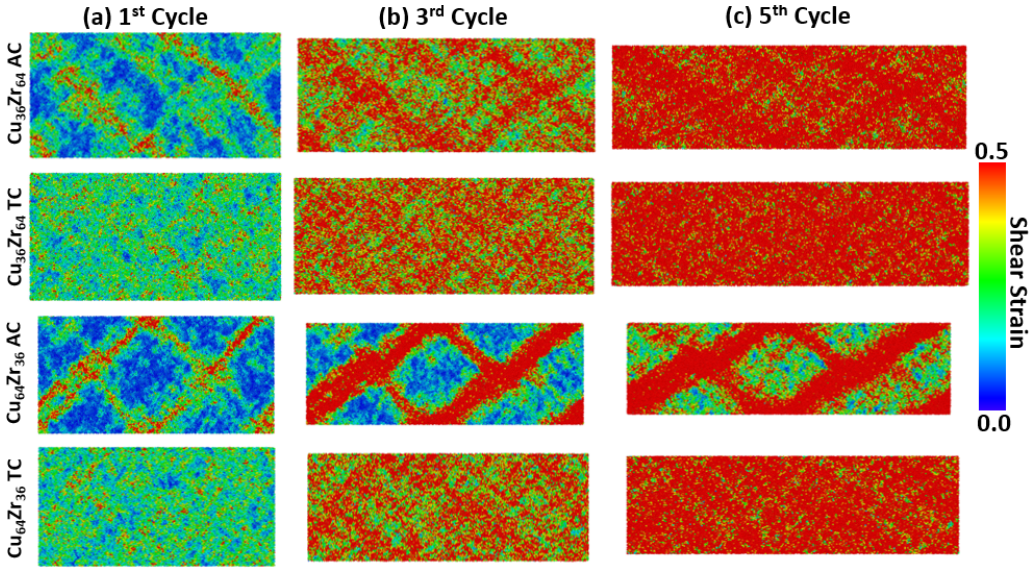

Figure 5. Atomic shear strain fields for the samples at the end of the 1st, 3rd, and 5th cycle.

Quantification of the plastic response was carried out using the degree of strain localization (ψ) and the participation ratio (ϕ), as shown in Figure 6. The sawtooth behavior in the curves corresponds to the unloading stage in each cycle. All curves converge to similar values, except for the AC Cu-rich MG, which shows localized deformation in the form of SBs [40,50–52]. In terms of the participation ratio, the other three samples quickly converge to 1.0, indicating that all atoms have undergone significant plastic activity, with shear strain exceeding 0.2. This suggests that further cyclic loading will not induce additional plastic events. Additionally, this also explains the reduction in toughness, making the material more prone to failure. This phenomenon is delayed in the AC Cu-rich sample, where plasticity is still dominated by SBs.

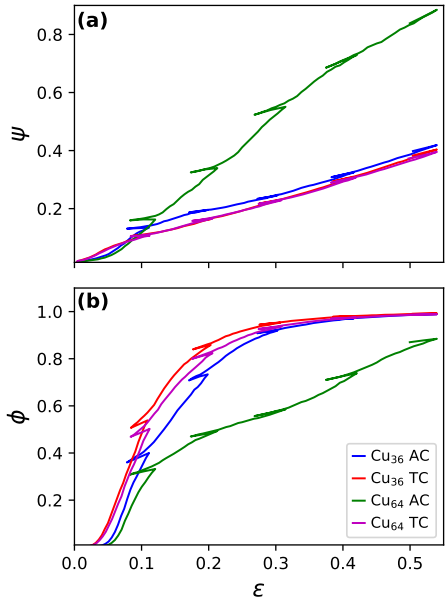

Figure 6. (**a**) Degree of strain localization and (**b**) participation ratio for each sample.

3.5. Variation of Structural Properties

Structural characterization was performed to gain further insights into the degradation of mechanical properties. The populations of solid-like polyhedra (F_s) and liquid-like polyhedra (F_l) [53,54], as well as the average fivefold local symmetry ($\overline{W}$) [31,55], were

calculated, with the results shown in Figure 7. Both TC and AC Cu-poor samples exhibit decreasing/increasing populations of solid-like/liquid-like polyhedra during the first and second cycles, followed by convergence to steady-state values, but with small variations, consistent with previous findings [14,18]. Interestingly, similar trends are observed in the AC Cu-rich sample, but to a greater extent, persisting up to the fifth cycle. A similar pattern is observed for $\overline{W}$, which is closely associated with solid-like polyhedra. These trends align with the participation ratio: while most atoms in the TC and AC Cu-poor samples undergo significant plastic activity after the second cycle, a large fraction of atoms in the AC Cu-rich sample still exhibit low atomic shear strain. Therefore, the AC Cu-rich sample can still undergo further structural transformations, unlike the other samples, which explains the more pronounced trends in polyhedra variations. A relevant question arises: Is there a threshold atomic composition at which the delayed behavior of the AC Cu-rich ceases to exist? Further studies are needed to clarify this.

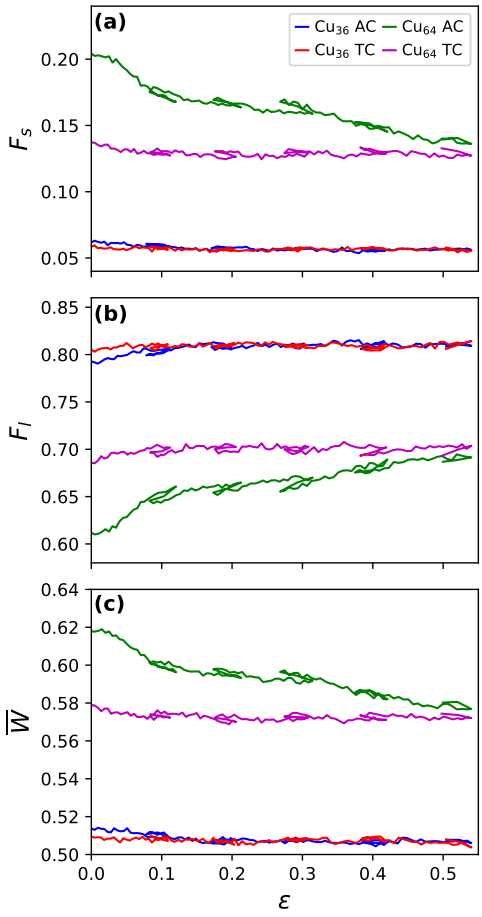

Figure 7. Variation of (**a**) solid-like polyhedra, (**b**) liquid-like polyhedra, and (**c**) average fivefold local symmetry during cyclic loading.

Additionally, the variation in per-atom potential energy U was calculated, as shown in Figure 8. In both TC samples, the initial potential energy is higher than in their AC counterparts, as expected from typical rejuvenation treatments [28,29,56,57]. In the case of the AC Cu-poor sample, cyclic loading rapidly increases U, converging to the curve of the TC Cu-poor case. A similar phenomenon is observed for the Cu-rich samples, though at a slower rate. This can be attributed to the large population of densely-packed Voronoi polyhedra in the AC Cu-rich sample, which provides more resistance to atomic rearrangement and, thus, to mechanical deformation [58–60]. Furthermore, it is worth noting that cyclic loading drives the samples to higher energy states, similar to reports

where rejuvenation was induced by mechanical deformation [11,15,61–64]. However, additional studies are required to further investigate this matter.

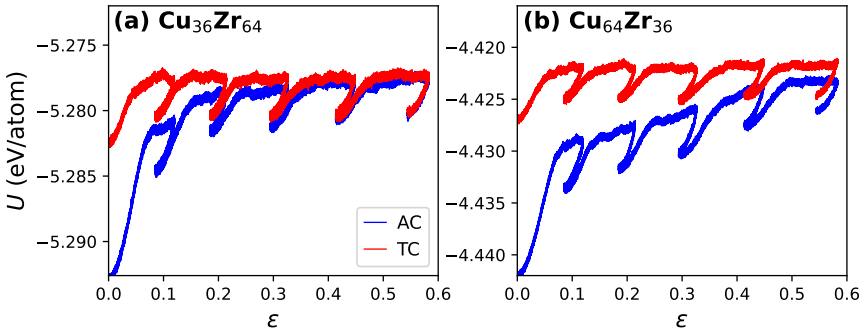

Figure 8. Variation of per-atom potential energy during cyclic loading.

4. Conclusions

This study explored the degradation of mechanical properties in CuZr metallic glasses (MGs) under cyclic loading using molecular dynamics simulations. Both $Cu_{36}Zr_{64}$ and $Cu_{64}Zr_{36}$ compositions were analyzed, considering as-cast (AC) and cryogenically thermal-cycled (TC) samples. The results reveal that cyclic loading leads to significant degradation in Young's modulus, ultimate tensile stress, and toughness in all samples, with the most pronounced decline occurring in the first few cycles. While AC samples exhibit higher initial mechanical performance, they experience a more severe reduction in properties, particularly in terms of ultimate tensile stress and toughness. In contrast, TC samples, which initially display lower strength due to rejuvenation effects, show more stable behavior during the later cycles, indicating that the structural changes induced by thermal cycling make them more resistant to fatigue-related degradation. Conducting additional deformation cycles could reveal whether the degradation of mechanical properties is a continuous process or converges to a steady state.

When comparing the two compositions, Cu-rich samples exhibit higher strength but similar degrees of degradation to Cu-poor samples. However, the AC Cu-rich sample demonstrates more localized plastic deformation in the form of shear bands, leading to delayed degradation compared to the more homogeneous deformation observed in the TC samples. Both TC and AC Cu-poor samples tend to reach a steady state more quickly, resulting in a faster degree of degradation compared to the AC Cu-rich MG. These findings suggest that while TC can enhance the ductility and stability of MGs under cyclic loading, the atomic composition plays a crucial role in determining both the extent and nature of degradation.

Funding: Project supported by the Competition for Research Regular Projects, year 2023, code LPR23-05, Universidad Tecnológica Metropolitana. Powered@NLHPC: This research was partially supported by the supercomputing infrastructure of the NLHPC (ECM-02).

Data Availability Statement: The data that support the findings of this study are available upon reasonable request from the author.

Conflicts of Interest: The author declares no conflicts of interest.

References

1. Johnson, W.L. Bulk metallic glasses—A new engineering material. *Curr. Opin. Solid State Mater. Sci.* **1996**, *1*, 383–386. [CrossRef]
2. Telford, M. The case for bulk metallic glass. *Mater. Today* **2004**, *7*, 36–43. [CrossRef]
3. Wang, W.H. Bulk Metallic Glasses with Functional Physical Properties. *Adv. Mater.* **2009**, *21*, 4524–4544. [CrossRef]
4. Kruzic, J.J. Bulk Metallic Glasses as Structural Materials: A Review. *Adv. Eng. Mater.* **2016**, *18*, 1308–1331. [CrossRef]
5. Gilbert, C.J.; Schroeder, V.; Ritchie, R.O. Mechanisms for fracture and fatigue-crack propagation in a bulk metallic glass. *Metall. Mater. Trans. A* **1999**, *30*, 1739–1753. [CrossRef]

6. Jia, H.; Wang, G.; Chen, S.; Gao, Y.; Li, W.; Liaw, P.K. Fatigue and fracture behavior of bulk metallic glasses and their composites. *Prog. Mater. Sci.* **2018**, *98*, 168–248. [CrossRef]
7. Sha, Z.; Lin, W.; Poh, L.H.; Xing, G.; Liu, Z.; Wang, T.; Gao, H. Fatigue of Metallic Glasses. *Appl. Mech. Rev.* **2020**, *72*, 050801. [CrossRef]
8. Wang, X.; Wu, S.; Qu, R.; Zhang, Z. Shear Band Evolution under Cyclic Loading and Fatigue Property in Metallic Glasses: A Brief Review. *Materials* **2021**, *14*, 3595. [CrossRef]
9. Louzguine-Luzgin, D.; Zadorozhnyy, V.Y.; Ketov, S.; Wang, Z.; Tsarkov, A.; Greer, A. On room-temperature quasi-elastic mechanical behaviour of bulk metallic glasses. *Acta Mater.* **2017**, *129*, 343–351. [CrossRef]
10. Ma, Z.C.; Ma, X.X.; Zhao, H.W.; Zhang, F.; Zhou, L.M.; Ren, L.Q. Novel Crystallization Behaviors of Zr-Based Metallic Glass Under Thermo-Mechanical Coupled Fatigue Loading Condition. *Acta Metall. Sin. (Engl. Lett.)* **2019**, *32*, 797–802. [CrossRef]
11. Li, S.; Huang, P.; Wang, F. Rejuvenation saturation upon cyclic elastic loading in metallic glass. *Comput. Mater. Sci.* **2019**, *166*, 318–325. [CrossRef]
12. Priezjev, N.V. Aging and rejuvenation during elastostatic loading of amorphous alloys: A molecular dynamics simulation study. *Comput. Mater. Sci.* **2019**, *168*, 125–130. [CrossRef]
13. Li, M.-f.; Wang, P.-w.; Malomo, B.; Yang, L. A scheme for achieving strength-ductility trade-off in metallic glasses. *Int. J. Plast.* **2023**, *169*, 103734. [CrossRef]
14. Bai, Y.; She, C. Atomic structure evolution in metallic glasses under cyclic deformation. *Comput. Mater. Sci.* **2019**, *169*, 109094. [CrossRef]
15. Priezjev, N.V. Fatigue Behavior of Cu-Zr Metallic Glasses under Cyclic Loading. *Metals* **2023**, *13*, 1606. [CrossRef]
16. Sha, Z.D.; Qu, S.X.; Liu, Z.S.; Wang, T.J.; Gao, H. Cyclic Deformation in Metallic Glasses. *Nano Lett.* **2015**, *15*, 7010–7015. [CrossRef] [PubMed]
17. Yang, M.H.; Li, J.H.; Liu, B.X. Comparatively studying the local atomic structures of metallic glasses upon cyclic-loading by computer simulations. *RSC Adv.* **2017**, *7*, 18358–18365. [CrossRef]
18. Shi, Y.; Louca, D.; Wang, G.; Liaw, P.K. Compression-compression fatigue study on model metallic glass nanowires by molecular dynamics simulations. *J. Appl. Phys.* **2011**, *110*, 023523. [CrossRef]
19. Mendelev, M.; Kramer, M.; Ott, R.; Sordelet, D.; Yagodin, D.; Popel, P. Development of suitable interatomic potentials for simulation of liquid and amorphous Cu–Zr alloys. *Philos. Mag.* **2009**, *89*, 967–987. [CrossRef]
20. Wakeda, M.; Saida, J. Heterogeneous structural changes correlated to local atomic order in thermal rejuvenation process of Cu-Zr metallic glass. *Sci. Technol. Adv. Mater.* **2019**, *20*, 632–642. [CrossRef] [PubMed]
21. Wang, J.; Liu, X.; Wu, Y.; Wang, H.; Ma, D.; Lu, Z. Clustering-mediated enhancement of glass-forming ability and plasticity in oxygen-minor-alloyed Zr-Cu metallic glasses. *Acta Mater.* **2023**, *261*, 119386. [CrossRef]
22. Zhang, J.; Zhang, M.; Wang, X.; Li, M. Gradient network architecture design induced strain delocalization and delayed failure in metallic glass matrix composites. *Scr. Mater.* **2023**, *237*, 115721. [CrossRef]
23. Amigo, N. Modulation of plasticity by crystalline precipitates in CuZr metallic glasses. *Mater. Today Commun.* **2024**, *39*, 109018. [CrossRef]
24. Plimpton, S. Fast Parallel Algorithms for Short-Range Molecular Dynamics. *J. Comput. Phys.* **1995**, *117*, 1039. [CrossRef]
25. Thompson, A.P.; Aktulga, H.M.; Berger, R.; Bolintineanu, D.S.; Brown, W.M.; Crozier, P.S.; in 't Veld, P.J.; Kohlmeyer, A.; Moore, S.G.; Nguyen, T.D.; et al. LAMMPS—A flexible simulation tool for particle-based materials modeling at the atomic, meso, and continuum scales. *Comp. Phys. Comm.* **2022**, *271*, 108171. [CrossRef]
26. Foroughi, A.; Ashuri, H.; Tavakoli, R.; Stoica, M.; Şopu, D.; Eckert, J. Structural modification through pressurized sub-Tg annealing of metallic glasses. *J. Appl. Phys.* **2017**, *122*, 215106. [CrossRef]
27. Moitzi, F.; Şopu, D.; Holec, D.; Perera, D.; Mousseau, N.; Eckert, J. Chemical bonding effects on the brittle-to-ductile transition in metallic glasses. *Acta Mater.* **2020**, *188*, 273–281. [CrossRef]
28. Shang, B.; Wang, W.; Greer, A.L.; Guan, P. Atomistic modelling of thermal-cycling rejuvenation in metallic glasses. *Acta Mater.* **2021**, *213*, 116952. [CrossRef]
29. Amigo, N. Cryogenic thermal cycling rejuvenation in metallic glasses: Structural and mechanical assessment. *J. Non-Cryst. Solids* **2022**, *596*, 121850. [CrossRef]
30. Peng, H.L.; Li, M.Z.; Wang, W.H. Structural Signature of Plastic Deformation in Metallic Glasses. *Phys. Rev. Lett.* **2011**, *106*, 135503. [CrossRef]
31. Hu, Y.C.; Li, F.X.; Li, M.Z.; Bai, H.Y.; Wang, W.H. Five-fold symmetry as indicator of dynamic arrest in metallic glass-forming liquids. *Nat. Commun.* **2015**, *6*, 8310. [CrossRef]
32. Shimizu, F.; Ogata, S.; Li, J. Theory of Shear Banding in Metallic Glasses and Molecular Dynamics Calculations. *Mater. Trans.* **2007**, *48*, 2923–2927. [CrossRef]
33. Stukowski, A. Visualization and analysis of atomistic simulation data with OVITO–the Open Visualization Tool. *Model. Simul. Mater. Sci. Eng.* **2010**, *18*, 015012. [CrossRef]
34. Cheng, Y.Q.; Cao, A.J.; Ma, E. Correlation between the elastic modulus and the intrinsic plastic behavior of metallic glasses: The roles of atomic configuration and alloy composition. *Acta Mater.* **2009**, *57*, 3253–3267. [CrossRef]

35. Shi, Y.; Falk, M.L. Strain Localization and Percolation of Stable Structure in Amorphous Solids. *Phys. Rev. Lett.* **2005**, *95*, 095502. [CrossRef]
36. Adibi, S.; Branicio, P.S.; Joshi, S.P. Suppression of Shear Banding and Transition to Necking and Homogeneous Flow in Nanoglass Nanopillars. *Sci. Rep.* **2015**, *5*, 15611. [CrossRef]
37. Cheng, Y.; Ma, E. Atomic-level structure and structure–property relationship in metallic glasses. *Prog. Mater. Sci.* **2011**, *56*, 379–473. [CrossRef]
38. Kartouzian, A.; Antonowicz, J.; Lünskens, T.; Lagogianni, A.; Heister, P.; Evangelakis, G.; Felici, R. Toward cluster-assembled metallic glasses. *Mater. Express* **2014**, *4*, 228–234. [CrossRef]
39. Antonowicz, J.; Pietnoczka, A.; Pękała, K.; Latuch, J.; Evangelakis, G.A. Local atomic order, electronic structure and electron transport properties of Cu-Zr metallic glasses. *J. Appl. Phys.* **2014**, *115*, 203714. [CrossRef]
40. Amigo, N. Characterization of Z cluster connectivity in CuZr metallic glasses. *J. Mol. Model.* **2024**, *30*, 184. [CrossRef]
41. Albe, K.; Ritter, Y.; Şopu, D. Enhancing the plasticity of metallic glasses: Shear band formation, nanocomposites and nanoglasses investigated by molecular dynamics simulations. *Mech. Mater.* **2013**, *67*, 94–103. [CrossRef]
42. Ritter, Y.; Albe, K. Chemical and topological order in shear bands of Cu64Zr36 and Cu36Zr64 glasses. *J. Appl. Phys.* **2012**, *111*, 103527. [CrossRef]
43. Zhong, C.; Zhang, H.; Cao, Q.; Wang, X.; Zhang, D.; Ramamurty, U.; Jiang, J. Size distribution of shear transformation zones and their evolution towards the formation of shear bands in metallic glasses. *J. Non-Cryst. Solids* **2016**, *445–446*, 61–68. [CrossRef]
44. Amigo, N.; Valencia, F.J. Species Content Effect on the Rejuvenation Degree of CuZr Metallic Glasses Under Thermal-Pressure Treatments. *Met. Mater. Int.* **2022**, *28*, 2068–2074. [CrossRef]
45. Feng, S.; Chan, K.; Zhao, L.; Pan, S.; Qi, L.; Wang, L.; Liu, R. Rejuvenation by weakening the medium range order in Zr46Cu46Al8 metallic glass with pressure preloading: A molecular dynamics simulation study. *Mater. Des.* **2018**, *158*, 248–255. [CrossRef]
46. Amigo, N. Structural and rheological properties of CuZrAl metallic glasses under pressure preloading. *Comput. Mater. Sci.* **2023**, *216*, 111819. [CrossRef]
47. Li, S.; Yu, Y.; Branicio, P.S.; Sha, Z.D. Effects of rejuvenation modes on the microstructures and mechanical properties of metallic glasses. *Mater. Today Commun.* **2023**, *36*, 106493. [CrossRef]
48. Park, K.W.; Fleury, E.; Seok, H.K.; Kim, Y.C. Deformation behaviors under tension and compression: Atomic simulation of Cu65Zr35 metallic glass. *Intermetallics* **2011**, *19*, 1168–1173. [CrossRef]
49. Yang, G.; Xu, B.; Kong, L.; Li, J.; Zhao, S. Size effects in Cu50Zr50 metallic glass films revealed by molecular dynamics simulations. *J. Alloys Compd.* **2016**, *688*, 88–95. [CrossRef]
50. Lin, W.H.; Teng, Y.; Sha, Z.D.; Yuan, S.Y.; Branicio, P.S. Mechanical properties of nanoporous metallic glasses: Insights from large-scale atomic simulations. *Int. J. Plast.* **2020**, *127*, 102657. [CrossRef]
51. Katakareddi, G.; Yedla, N. The effect of loading methods on the microstructural evolution and degree of strain localization in Cu50Zr50 metallic glass composite nanowires: A molecular dynamics simulation study. *J. Mol. Graph. Model.* **2022**, *115*, 108216. [CrossRef] [PubMed]
52. Zhang, Y.; Cheng, M.; Meng, L.; Yao, X. Microstructural evolution of shear bands formation of metallic glasses under different loading conditions and strain rates. *J. Non-Cryst. Solids* **2022**, *584*, 121525. [CrossRef]
53. Wang, B.; Luo, L.; Guo, E.; Su, Y.; Wang, M.; Ritchie, R.O.; Dong, F.; Wang, L.; Guo, J.; Fu, H. Nanometer-scale gradient atomic packing structure surrounding soft spots in metallic glasses. *Npj Comput. Mater.* **2018**, *4*, 41. [CrossRef]
54. Wang, B.; Luo, L.; Dong, F.; Wang, L.; Wang, H.; Wang, F.; Luo, L.; Su, B.; Su, Y.; Guo, J.; et al. Impact of hydrogen microalloying on the mechanical behavior of Zr-bearing metallic glasses: A molecular dynamics study. *J. Mater. Sci. Technol.* **2020**, *45*, 198–206. [CrossRef]
55. Xie, L.; An, H.; Peng, Q.; Qin, Q.; Zhang, Y. Sensitive Five-Fold Local Symmetry to Kinetic Energy of Depositing Atoms in Cu-Zr Thin Film Growth. *Materials* **2018**, *11*, 2548. [CrossRef]
56. Amigo, N.; Valencia, F. Mechanical and structural assessment of CuZr metallic glasses rejuvenated by thermal-pressure treatments. *Comput. Mater. Sci.* **2021**, *198*, 110681. [CrossRef]
57. Li, H.; Jin, C.G.; Sha, Z.D. The effect of pressure-promoted thermal rejuvenation on the fracture energy of metallic glasses. *J. Non-Cryst. Solids* **2022**, *590*, 121674. [CrossRef]
58. Zaccone, A.; Scossa-Romano, E. Approximate analytical description of the nonaffine response of amorphous solids. *Phys. Rev. B* **2011**, *83*, 184205. [CrossRef]
59. Antonowicz, J.; Pietnoczka, A.; Evangelakis, G.A.; Mathon, O.; Kantor, I.; Pascarelli, S.; Kartouzian, A.; Shinmei, T.; Irifune, T. Atomic-level mechanism of elastic deformation in the Zr-Cu metallic glass. *Phys. Rev. B* **2016**, *93*, 144115. [CrossRef]
60. Milkus, R.; Zaccone, A. Local inversion-symmetry breaking controls the boson peak in glasses and crystals. *Phys. Rev. B* **2016**, *93*, 094204. [CrossRef]
61. Ross, P.; Küchemann, S.; Derlet, P.M.; Yu, H.; Arnold, W.; Liaw, P.; Samwer, K.; Maaß, R. Linking macroscopic rejuvenation to nano-elastic fluctuations in a metallic glass. *Acta Mater.* **2017**, *138*, 111–118. [CrossRef]
62. Pan, J.; Wang, Y.X.; Guo, Q.; Zhang, D.; Greer, A.L.; Li, Y. Extreme rejuvenation and softening in a bulk metallic glass. *Nat. Commun.* **2018**, *9*, 560. [CrossRef] [PubMed]

63. Zhang, L.; Wang, Y.; Pineda, E.; Yang, Y.; Qiao, J. Achieving structural rejuvenation in metallic glass by modulating B relaxation intensity via easy-to-operate mechanical cycling. *Int. J. Plast.* **2022**, *157*, 103402. [CrossRef]
64. Zhang, S.; Zhou, W.; Song, L.; Huo, J.; Yao, J.; Wang, J.; Li, Y. Decoupling between enthalpy and mechanical properties in rejuvenated metallic glass. *Scr. Mater.* **2023**, *223*, 115056. [CrossRef]